Comparison study between two different precursors of RGO/AuNPs one pot synthesis

Nurul Farhana Abu Kasim[1], Norhana Abdul Halim[2], Ong Keat Khim[2] and Siti Zulaikha Ngah Demon[2]

[1]Faculty for Defence Science and Technology, National Defence University of Malaysia, Sungai Besi Camp, 57000 Sungai Besi, Kuala Lumpur, Malaysia

[2]Centre for Defence Foundation Studies, National Defence University of Malaysia, Sungai Besi Camp, 57000 Sungai Besi, Kuala Lumpur, Malaysia

Email : zulaikha@upnm.edu.my

Abstract. One pot synthesis of graphene nanocomposites is low-cost and time-efficient methodology to be considered for large scale device fabrication. Graphene precursors made of renewable and waste materials such as rice husk, oil palm kernel and sugar are explored upon rising concern of expensive and hazard in conventional approaches. This paper present chemical characterization study of one pot reduced graphene oxide/gold nanoparticles (RGO/AuNPs) synthesized from low-cost sucrose as precursor and dehydroascorbic acid as green reducing agent at ambient condition which was originally used by Hurtado *et al* in 2020. Raman spectra of RGO/AuNPs was compared to composite of

commercial GO precursor to evaluate quality of reduction products. Result from UV-vis, FTIR and XPS spectroscopies showed both techniques successfully eliminated oxygen-containing functional groups to form graphene constitution. Asides from lower stability, AuNPs in sucrose-derived RGO possessed larger size and more dispersed than that of GO-derived RGO implying the need to optimize the current recipe. Reduction mechanism of both precursors was proposed for better understanding. The aim of this work is to show feasibility of green graphene nanocomposites synthesis that could empower productivity of electronic, optical and optoelectronics applications.

Keywords: Reduced graphene oxide, one-step reduction, gold nanoparticles, ascorbic acid, chemical

Classification numbers: 5.15

1. Introduction

Graphene is an ideal nanomaterial owing to its high crystallinity, flexibility, and excellent conductivity. Optimized graphene can be obtained via both bottom-up and top-down approaches such as chemical vapour deposition (CVD), mechanical and chemical exfoliation methods. Most common pathway is graphene oxide (GO) reduction where GO was initially produced via oxidation of graphite or other carbon sources and subsequently reduced to obtain graphene. It is less complicated than CVD graphene despite involving hazardous chemicals [1]. The oxygen functional groups of GO make it processable in polar solvent i.e water, hence, can be easily integrated and transferable into film devices [2]. Graphene-based nanocomposites are explored due to strength, thermal and electrical improvement of material when graphene is added as filler. While conductivity of GO varied from an insulator to a semiconductor depending on precursor and synthesis environment, reduced graphene oxide (RGO) will restore electronic superiority of pristine graphene [2]. Being less susceptible to graphene sheets stacking, the increase of surface area of partially oxygenated RGO makes it advantageous in the making of effective electrochemical sensors [3], energy storage electrodes [4] and other devices [5].

Availability of many reduction methods such as thermal and chemical ways can produced various quality of RGO that can be assessed by the amount of carbon to oxygen (C:O) ratio [6], preference for removal of each oxygen functional groups [7], surface defects [8], and reducing agent selection [9]. In

chemical reduction of GO, hydrazine's hazard can be avoided by employing green reductants such as ascorbic acid [10-11], green tea [12], and various plant extract [13]. It was found that RGO by ascorbic acid (AA, a form of vitamin C) produced comparable structural quality to those synthesized by hydrazine [14]. AA reduction process can also be carried out in water. Effective use of AA has been shown by Xu *et al* where electrical conductivity attained by RGO reduced AA is the highest among obtained from glucose and tea polyphenol reductants [15].

Hydroxyl (-OH), epoxy (C-O-C), carbonyl (C=O) and carboxylic acid (-COOH) on GO's surfaces and edges provides less Van der Waals interaction among graphene sheets, creating high surface area per volume matrixes for anchoring high load of nanoparticles and biomaterials in one-pot synthesis or one-step reduction approaches [2]. Hydrazine's and AA's not only disperse, stabilize but also promote graphene interaction with nanoparticles in which enhancement of electronic and optical phenomenon such as luminescence and surface plasmon resonance (SPR) are feasible. In one study, it was demonstrated introduction of RGO/AgNPs coating enhanced the SPR signal by 150% and prevented the AgNPs from oxidizing during detection [16].

On the other hand, three-dimensional carbon precursors derived from organic waste such as oil palm [17], sugar beet bagasse [18], rice husk [19], and coconut shell [20] have been reportedly used to synthesize graphene and carbon nanomaterials. These carbon sources are cheap and sustainable alternative but

required carbonization process and treatment steps to become graphene derivatives. Herein, we present some chemical characterization studies of one-step RGO/AuNPs preparation using GO and sucrose as RGO precursors. Reducing agents of AA and dehydroascorbic acid (DHA, a form of oxidized AA) are used for each precursor, respectively. The later recipe was featured in report by Hurtado *et al* for SERS application and will be used as discussion in this paper [21]. Our objectives are to contribute deeper understanding in the reduction mechanism, chemical characteristics and the end-product quality of different carbon precursors in RGO/AuNPs green synthesis.

2. Experimental

2.1. *Materials*

Graphene oxide (GO dispersion in H_2O, 4 mg/ml), sucrose (≥ 99.5%), dehydroascorbic acid (quality level 200, DHA), gold (III) chloride hydrate (99.995% trace metal basis, $HAuCl_4$), and ascorbic acid (99%, AA) were purchased from Sigma Aldrich. Deionized water was prepared by a Milli-Q Plus system (Millipore).

2.2. *Synthesis of ascorbic acid reduced graphene oxide/Au nanoparticles (RGO-AA/AuNPs)*

GO solution was prepared by sonication method. Firstly, 2.5 ml of GO dispersion were added into 97.5 ml of deionized water and sonicated for 30 minutes, designated as solution S1. 1 ml of $HAuCl_4$ (0.01M) was added into 20 ml

deionized water and stirred manually for few seconds, designated as solution S2. 30 mg of AA was then added into combined mixture of S1 and S2. After that, the solution was heated to 95°C and kept for 90 min under vigorous stirring, resulting in RGO-AA/AuNPs. Successful reduction was indicated by colour change from brownish to light purple due to presence of gold nanoparticles. The solution was then centrifuged to remove excess GO flakes.

2.3. *Synthesis of dehydroascorbic acid reduced graphene oxide/Au nanoparticles (RGO-DHA/AuNPs)*

RGO-DHA/AuNPs was synthesized in similar manner reported by Hurtado *et al* [21]. Firstly, 0.25 g sucrose was added into 40 ml deionized water mixed with 40 ml of 0.05 M DHA. The solution was sonicated for 30 minutes and designated as solution S1. Solution S2, the gold precursor was prepared using 0.01 M of $HAuCl_4$ in deionized water. Both solutions were diluted as follows; 1 ml of S2 was added into 20 ml deionized water, meanwhile 0.5 ml of S1 was diluted in 10 ml deionized water. They were mixed and stirred for 20 min at ambient temperature. The colour changed from opaque yellow to blueish purple signified formations of both RGO and gold nanoparticles. Both synthesis of RGO/AuNPs were summarized in Figure 1.

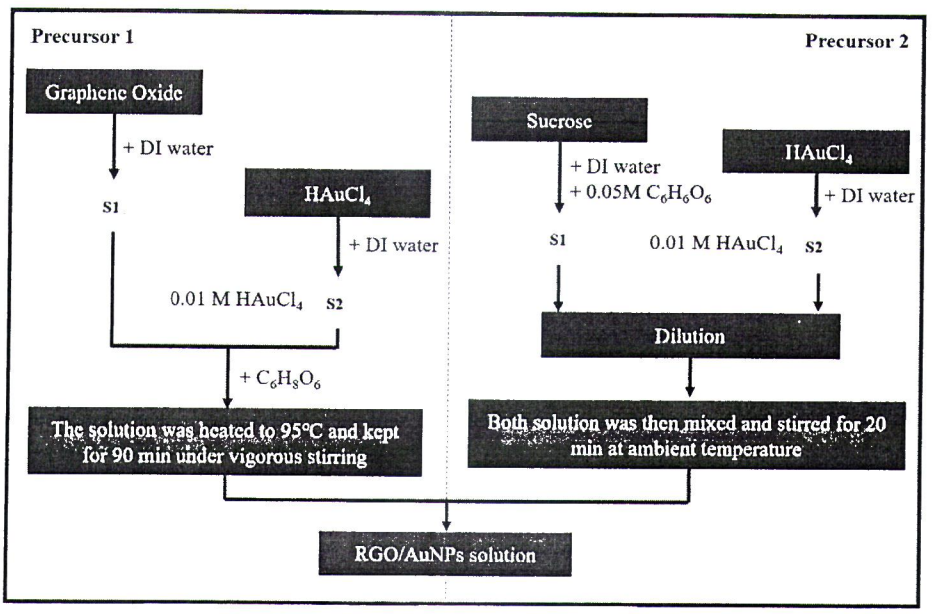

Figure 1. Scheme for the synthesis of RGO/AuNPs using graphene oxide and sucrose as precursors.

2.4. *Characterization*

Material characterizations were provided by UV-Vis spectroscopy, High resolution transmission electron microscopy (HR-TEM), particle analyser, X-ray photoelectron spectrometer (XPS), Fourier-transform infrared spectroscopy (FTIR) and Raman spectrometer of Perkin Elmer Lambda 19, Technai G2 20 X-Twin, Antonn Parr Litesizer 500, Shimadzu Axis Ultra DLD, Perkin Elmer Frontier IR, and Agilent Resolve Raman System, respectively. HR-TEM was operated at 200 kV accelerating voltage and the morphology analysis was conducted using ImageJ software. XPS was carried out with a spherical mirror analyser (Mg and Al K-alpha X-ray sources). The following pass energy values were used: 187.85 eV for survey spectra and 23.5 eV for high-resolution scans.

A combined electron and argon ion gun neutralizer system was used for charge compensation during the acquisitions. The analysis of experimental data was performed with CasaXPS and Origin software. The binding energy scale was calibrated by placing the C–C sp^2 component at 284.5 eV as provided in Origin. The FTIR study was carried out with ATR accessory in the mid IR range. The excitation line for Raman measurement is 830 nm, 475 mW and all spectra were collected in back scattering geometry. All data was used to explain graphene and gold nanoparticles transformations in term of chemical bonding and quality of the nanocomposites.

3. Result and discussion

3.1. *Validation of RGO/AuNPs reduction*

Figure 2 (a-b) shows absorption spectra of precursors and their respective final reduction product, the RGO/AuNPs. They will be used to validate reduction processes of GO and sucrose by observing signatures peak related to RGO and AuNPs. Firstly, RGO formations were validated by GO's absorption peak shifting from 234 nm to 246 nm in RGO-AA/AuNPs spectrum and materialization of RGO peak at 250 nm in RGO-DHA/AuNPs spectrum. These peaks correspond to π-π^* transition related to C=C bond in an aromatic ring of the graphene and their observation is a strong indicator for RGO [18, 22]. The intensity of RGO peak in Fig. 2 (b) is comparatively smaller implying there are low percentage of RGO compared to sucrose precursor present in the measured

sample. It was seen that SPR peak of RGO-DHA/AuNPs located at a longer wavelength, 566 nm compared to SPR peak of AA-reduced composite which is positioned at 554 nm. The former also appeared to be broader.

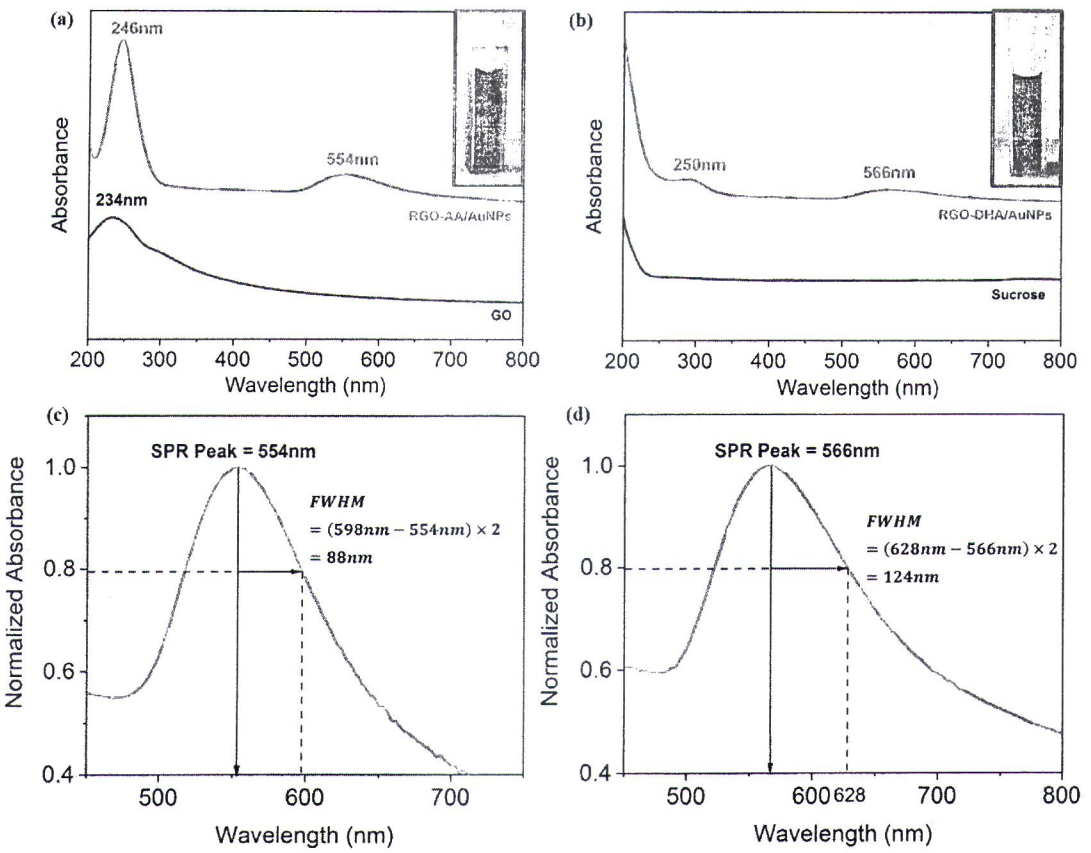

Figure 2. UV-Vis absorbance and normalized SPR spectra of (a,c) RGO-AA/AuNPs and (b,d) RGO-DHA/AuNPs samples in solutions.

According to Rizzi *et al*, theoretical grain size of AuNPs as 37 nm and 42 nm for RGO-AA/AuNPs and RGO-DHA/AuNPs, respectively [23]. These estimated size of AuNPs for RGO-AA/AuNPs is consistent with HR-TEM observation in Fig. 3 as spherical nanoparticles were found to be randomly anchored on RGO

templates [24]. Full wave half maximum (FWHM) of SPR peaks is shown in Fig. 2 (c-d). The analysis is used to estimate dispersity of the AuNP clusters with larger FHWM value indicating more dispersed particles. Clearly, not only the average size of AuNPs in DHA reduction product is higher than that of AA reduction product, but they are more distanced from each other as well. The reason for the separation is because of insufficient anchoring by sucrose derived RGO. Unlike 1D and 2D graphene structure of GO and RGO shown in Fig. 3 (a-b), the sucrose precursor did not pre-exist as graphene sheets as has been previously measured by Hurtado *et al* [21]. It is a well-known fact that the AuNPs morphology is influenced by the type of reducing agents and precursor materials [25]. Fig. 3 (d-e) shows variation of AuNPs size analysis of single AuNPs reduction and the one pot composite reduction. The hydrodynamic diameter obtained in RGO-DHA/AuNPs is 87.21 ± 0.91 nm (polydispersity index 20.3%) which is higher than pristine AuNPs sample at 52.83 ± 0.61 nm (polydispersity index 28.1%). Since the AuNPs are physically adsorbed on carbon templates, it makes sense that the diameter measured from light scattering methodology is higher for composite.

Other than that, experiment of storage stability showed that AA reduced composite is stable up to 30 days in chilled environment, whereas DHA reduced composite showed rapid change from purple to colourless after 2 days and on the third day, the AuNPs precipitated at the bottom of the vials. This fast degradation

emphasized the weakness of current recipe hence encouraging the immobilization of RGO-DHA/AuNPs on substrates as soon it is processed.

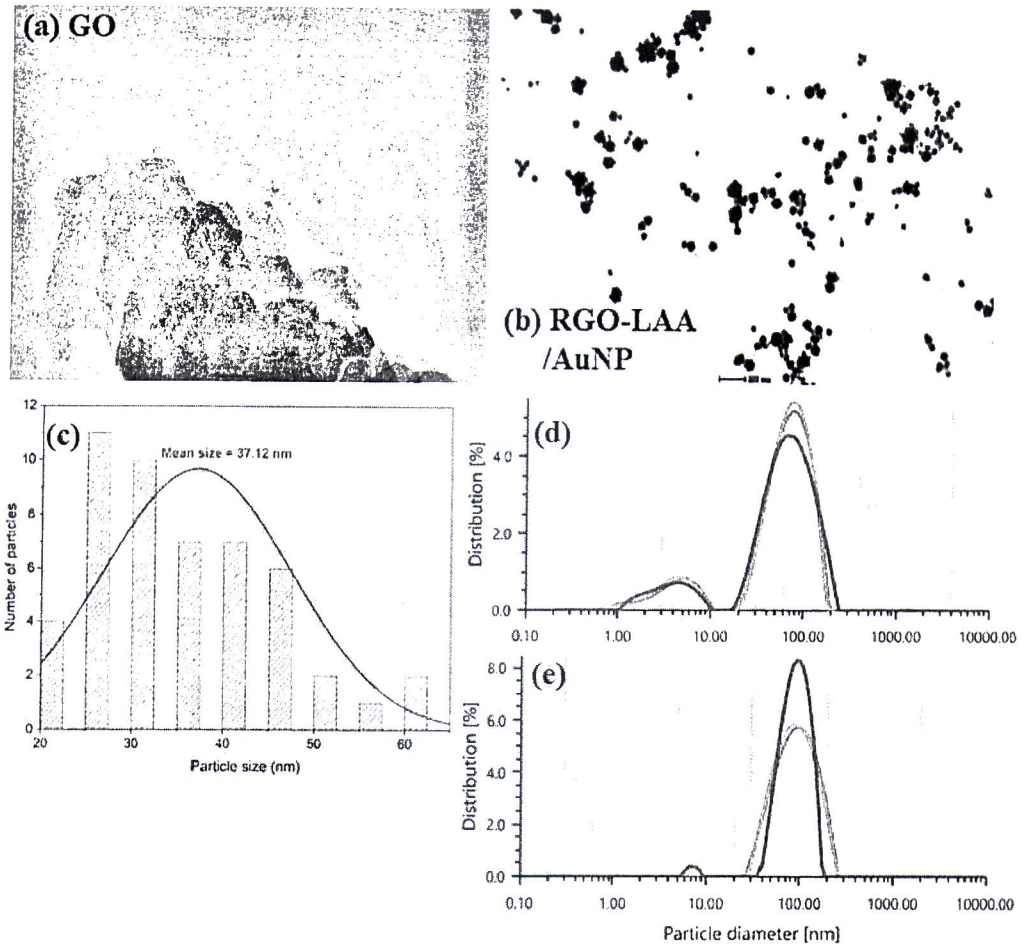

Figure 3. (a-b) HR-TEM images of GO and RGO-AA/AuNPs, (c) size distribution histograms of AuNPs for RGO-AA/AuNPs. Particle size distribution analysis of (d) AuNPs and (e) RGO-DHA/AuNPs for comparison.

3.2. *Chemical reduction degree of RGO/AuNPs by XPS*

XPS spectra was used to evaluate chemical reduction degree and as standardized carbon materials, the C 1s peak will be fitted and further analysed. Figure 4 shows the chemical compositional percentage for (a) GO as precursor and (b) end-

product, RGO-AA/AuNPs deposited on quartz substrates. XPS spectra of GO consists of significant contribution from 41.13 % C and 58.87 % O, while RGO-AA/AuNPs show 11.66 % composition from Au, asides from 33.77 % C, 54.21 % O which proved generation of AuNPs in the composite. The deconvoluted high-resolution C 1s of GO and RGO-AA/AuNPs are displayed in Fig. 4 (c, d). The high-resolution C 1s spectrum of GO exhibited a saddle-like pattern, which is a signature of extreme oxidization in GO.

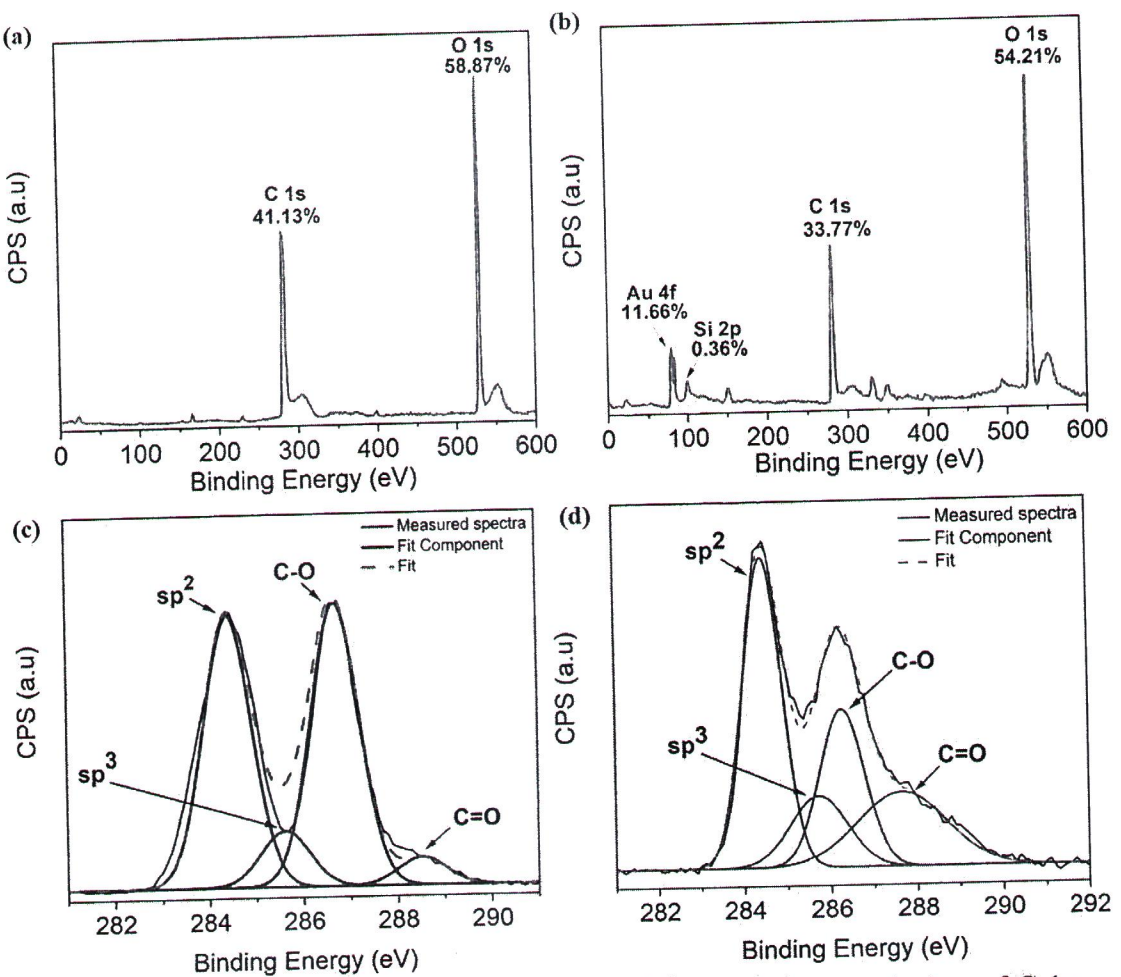

Figure 4. XPS spectra of the chemical composition and deconvolution of C 1s for (a, c) GO and (b, d) RGO-AA/AuNPs.

GO is an atomically thin sheet of carbon covalently bonded to several oxygen functional groups thus producing sp^2 and sp^3 hybridized carbon atoms [26]. In addition to the sp^2 graphitic component and sp^3 hybridization, deconvolution of the C 1s peak in GO discloses peaks of oxygen-carrying functional groups. The component at 287 eV is assigned to C atoms directly bonded to oxygen (hydroxyl and epoxy configurations), whereas the component at 288.8 eV is assigned to carbonyl groups. The commercially obtained GO possessed almost equivalent contribution of sp^2 carbons and the C-O bonds. Intensity of these peaks changed after reduction of GO in AA was performed. As a result, intensities of the C-O groups remarkably decreased by 47.67% from it was previously and sp^2 contribution becomes more dominant which suggested the GO were successfully reduced [27]. Transformation from double peak spectra to single sharp peak toward low binding energies is indicative of graphene configuration [28]. The result implied that the hydroxyl and epoxide groups populating graphene basal plane are strongly affected by AA removal, compared to the carbonyl groups which resided on edges of graphene sheets.

On the other hand, Fig. 5 shows XPS spectra analysis of sucrose reduction by dehydroascorbic acid. Sucrose as carbon precursor also mainly consisted of carbon and oxygen, each at 30.88 % and 69.12 %. In Fig. 5(c), sucrose exhibits lowest non-oxygenated C 1s intensity the sp^2 (peak centred at 284.5 eV) caused by atmospheric contamination of the sugar at C-C bonds [29]. After reduction by DHA, the sp^2 becomes more prominent which is a sign of extended carbon

backbone formation. The oxygenated C as sp^3 (peak at 286.8 eV) also decreased drastically after reduction process due to the lower oxygen functionality. The deformation also accompanied by decreased intensities from oxidized carbon groups such as C-O and C=O groups. From C 1s spectrum analysis, there is consistent pattern of reduction transformation between GO and sucrose precursors meaning that the sucrose derived RGO also leaned toward graphene bonding configuration [28]. One notable difference from this XPS comparison is that the intensity of sp^3 is relatively higher than the oxidized groups for RGO-DHA/AuNPs.

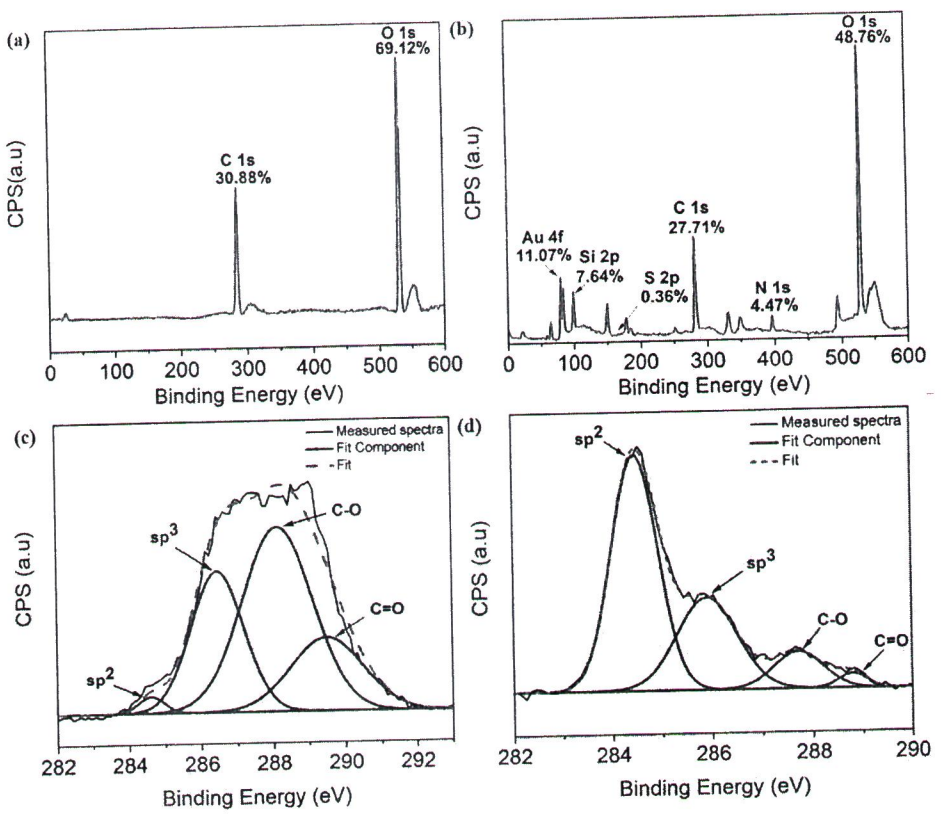

Figure 5. XPS spectra of the chemical composition and deconvolution of C 1s for (a, c) sucrose and (b, d) RGO-DHA/AuNPs.

3.3. *Raman and FTIR spectra of RGO/AuNPs nanocomposites*

FTIR spectra of precursor materials and their reduction products, the RGO/AuNP nanocomposites are used to obtain more insights on oxygen functional group transformation. In Fig. 6 (a), both GO and RGO-AA/AuNPs spectra demonstrate vibrational modes belonging to different oxygen functional groups of GO; the 1258 cm^{-1} peak for C–O–C bond, the 1670 cm^{-1} peak for C=O and the 3366 cm^{-1} peak for O–H bond. Transmittance decrease of these peaks are typical sign of deoxygenated graphene [30], but in our case, the AuNP physical substitutions maybe the reason behind the suppression of these signals. Nevertheless, it is seen that the epoxide group related vibrational mode has significantly reduced in RGO-AA/AuNPs compared to carbonyl group's, consistent with the XPS spectra observation. On the other hand, FTIR transformation shown in Fig. 6(b) are similar to one previously reported [21]. The FTIR characteristics consist of two distinct features of O-H stretching and C-C vibrational modes at approximately 3338 cm^{-1} and 1636 cm^{-1}, respectively. The broad hydroxyl peak is possibly contributed to the presence of DHA degradation products which is guluronic acid, that will be discussed in the next section [31]. Nevertheless, it was agreed that some notable peaks assigned to sucrose, for example the C-H bond, diminished upon reduction which suggested its transformation to graphene-like structure.

Figure 6(c) shows D and G bands obtained from GO, RGO-AA and RGO-AA/AuNPs indicating presence for graphitic structures in both samples. The ratio of these bands (I_D/I_G) increased from 0.93 to 1.06 when GO successfully reduced and increased to 1.28 after AuNPs occupied graphene surface defects. D band that represents disorder in sp^2 carbon network increases because of smaller average size of sp^2 domains (in the case of RGO) and presence of AuNPs in between the graphene layers during the co-reduction (in the case of composite). On the other hand, both Raman spectra of RGO-DHA and RGO-DHA/AuNPs in Fig. 6(d) shows presence of G band, each centred at ~1590 cm^{-1} and ~1530 cm^{-1} . Low defect ratio of 0.42 is calculated for RGO-DHA sample and strong appearance of broad peak at 1460 cm^{-1} corresponding to amorphous carbon phases or the D' band [32-33]. For RGO-DHA/AuNPs, two prominent peaks already denoted as D' and G bands are observed at ~1440 cm^{-1} and ~1530 cm^{-1}, respectively. These two peaks become prominent to explain formation of sp-sp^2 carbon sheets of graphene derivatives [33]. The ratio of these bands is calculated as 1.46. Shift of graphene's G band in Fig. 6(d) can be attributed to defect contribution as explained by King *et al* [34].

3.4. *Proposed reduction mechanism of RGO/AuNPs*

Understandably, application of synthetic chemical and toxic precursor materials will lead to higher manufacturing cost. Hence, using sucrose as graphene

precursor will provide alternative to Hummer's GO and to be able to process RGO at ambient condition will be an advantage in research works. The ascorbic

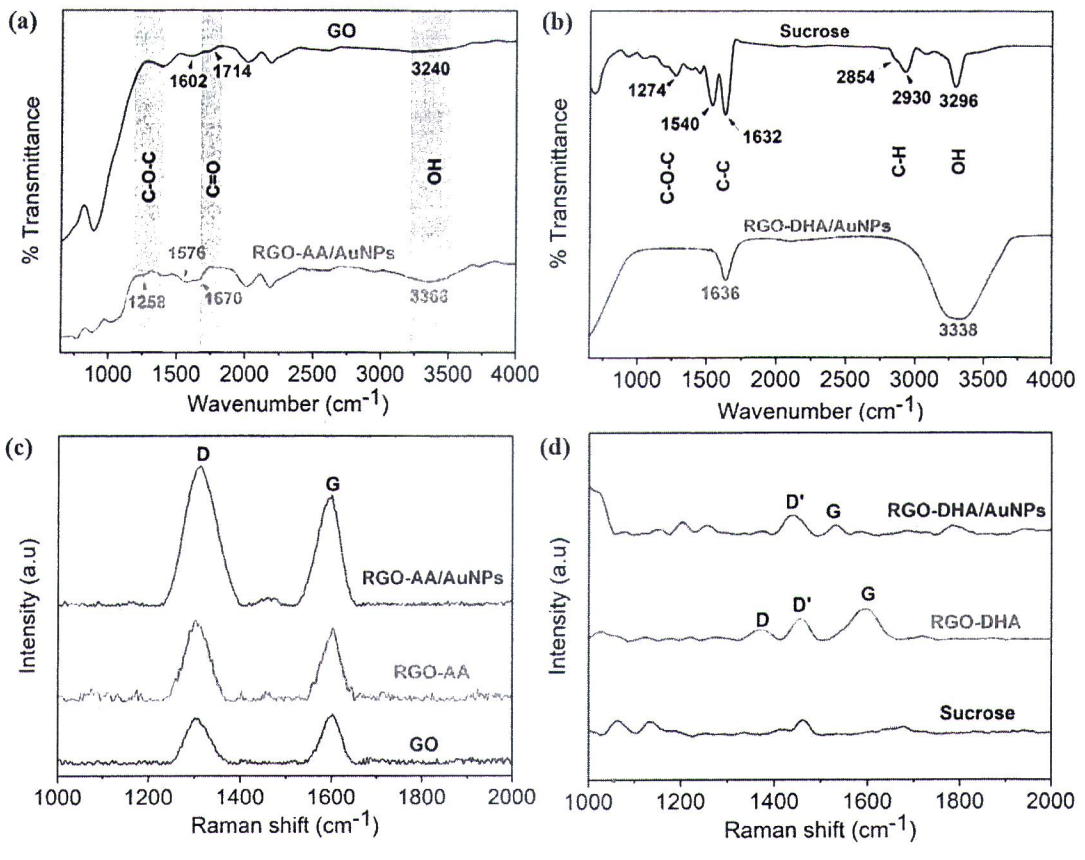

Figure 6. (a-b) FTIR spectra of (a) RGO-AA/AuNPs and (b) RGO-DHA/AuNPs with their precursors. (c-d) Raman spectra of (c) RGO-AA/AuNPs and (d) RGO-DHA/AuNPs with their precursors.

acid reduction mechanism from GO to RGO has been established elsewhere [35]. It basically involved two-step nucleophilic reactions followed by one-step of thermal elimination of epoxy and hydroxyl groups as illustrated in Fig. 7. As a result, AA will oxidize into dehydroascorbic acid and water molecules as by-products. This conclusion is in well agreement with our XPS and FTIR findings.

Meanwhile, a little is known about reduction mechanism for both RGO-DHA/AuNPs other than the by-products of sucrose reduction to RGO are guluronic and oxalic acids [36]. Our result also indicated that the original chemical structure C–O–C and C–H of sucrose is affected by DHA reduction which explains their diminished contributions in XPS and FTIR.

During this simultaneous reduction of carbon material and $HAuCl_4$, AA and DHA are antioxidants phytoconstituents capable of reducing Au^{3+} ions on the surface of the RGO by donating electrons or hydrogen atoms, effectively forming Au^0 particles [27]. As GO sheets were reduced, the metal ions were also adsorbed on graphene surface defects effectively preventing their reaggregation and restacking, resulting into longer shelf life of the nanocomposite colloid [27]. The same stability could not be said for RGO-DHA/AuNPs due to insufficient anchoring by carbon templates. While our result implied that DHA reduced RGO has structure resembled of graphene and combined sp-sp^2 carbon structure, it is most likely amorphous and consist of unregulated areas and lengths. Our hypothesis is that the structural difference and stronger RGOs interaction are the reason that AuNPs could not be properly anchored on their surface.

The viability of this type of reduction is then compared with some excellent graphene and graphene nanocomposites synthesis studies of biomass and sustainable carbon precursors. Table 1 listed precursors materials, synthesis methods and notable findings of some graphene and graphene nanocomposites

studies. Research works shown in Ref. 25-28 employed the 'gold standard' of graphene synthesis which involved high temperature carbonization and GO's

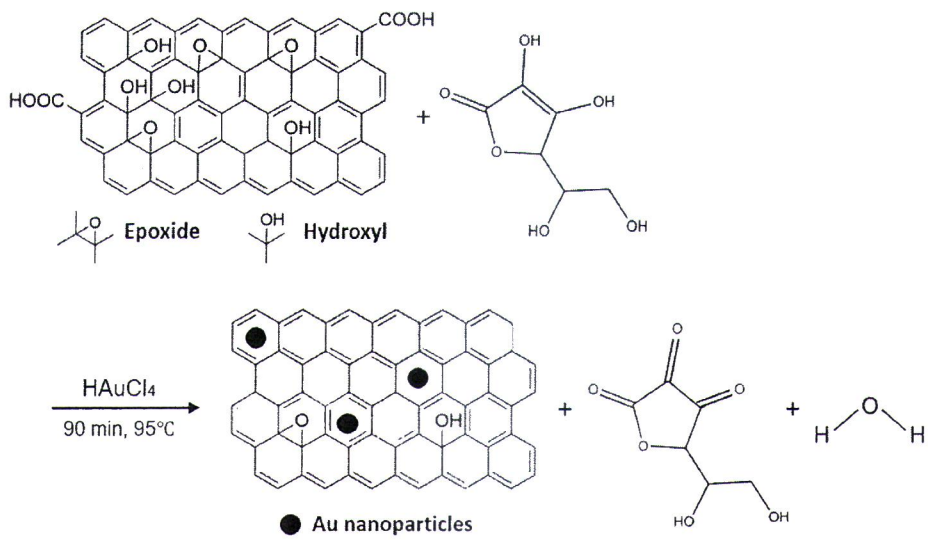

Figure 7. Reduction mechanism for Au decorated RGO for GO precursor.

Hummers which guaranteed excellent graphene quality as confirmed by either XRD, electron images or Raman characterizations [17-20]. Recently, Yousefimehr and his co-workers demonstrated green synthesis of RGO/AuNPs from biomass *B. oleracea* plant in a safer and milder environment compared to those former works [37]. Their work promoted the possibility of easy, fast, cost-effective and totally green approach in graphene synthesis. Featuring sucrose as RGO precursor and dehydroascorbic acid as reducing agent, our study promoted ambient processing of graphene. The sucrose derived RGO can be best described as laminates instead of sheets [21]. Its processing was found not only affect

physical properties of AuNPs but also the way the graphene nanocomposite can be immobilized as this type of precursor is more suitable for thin film coating applications.

Table 1. Precursors, synthesis method and notable findings of some graphene and graphene nanocomposites studies

Carbon precursor	Reducing agent	Synthesis method	Graphene quality assessment	Ref.
Oil palm waste	-	Pyrolysis/carbonization for 3 h at 400 - 900 °C. GO was then reduced by low-temperature annealing at 300 °C under N_2 for 1 h. Some hazardous chemicals were used.	• Prominent G-band with I_G/I_D varied from 1.06 - 1.20. • Carbon yield rate decreased as the carbonization temperatures increased. • Graphitic (002) planes at $2\Phi = 23.6°$. • Both microporous and nanoporous graphenes.	17
Sugar beet bagasse	$NaBH_4$	Combustion at 450 – 500 °C for 5 d. Next, grounded into powder and heated again at 450 °C for 24 h. Graphite powder obtained after 6 d evaporation before further modification by Hummer's method One pot reduction of $AgNO_3$ and GO using $NaBH_4$.	• RGO's XRD peak at $2\theta = 21.79°$. • The average size of AgNPs is17 nm. • Long shelf life at 395 d. • GO consists of thin wavy shape sheets with a porous fluffy network like a loose sponge.	18
Coconut shell waste	-	Carbonized at 600 °C for 3. Sample was washed with HF and stirred at 45 °C for 3 h. Then, washed again with alkaline, and oven dried at 110 °C for 12 h. GO obtained by modified Hummer's method.	• I_D/I_G was 0.89 and confirmed to be 2D single layer graphene. • Surface morphology consisted of abundance granular particles with different size distributions. • Semiconducting with E_G of 4.38 eV.	19
Rice husks	-	Carbonization followed by a one-stage KOH-activation.	• I_D/I_G and I_{2D}/I_G values are 0.953 and 0.36, respectively. • Nanosheets exhibited an ultra-thin crumpled-silk-veil-wave, sheet-like structure with a high surface area of ~1225 $m^2 g^{-1}$ and porosity.	20

			• The graphene electrode shows higher energy density compared to electrode of graphite and black soybeans precursors.	
Brassica oleracea stem	*Brassica oleracea* extract	Biomass powder was microwaved (900 W, 30 min) and autoclaved at 180 °C for 15 h. After wash and vacuum dried, one-pot synthesis was performed at 140 °C for 5 h.	• RGO's (002) crystal plane identified at 24.85°. • I_D/I_G ratios for RGO and AuNP/RGO were 0.99 and 0.81, respectively. • Average AuNPs size is ~24 nm.	36
Sucrose	Dehydroascorbic acid	One pot 20 min stirring at 25°C	• SEM images show RGO laminates with (101) crystal plane. • I_D/I_G for RGO/AuNP is 1.6. • Average AuNPs size is 15-30 nm.	21
Sucrose and GO	Dehydroascorbic acid and ascorbic acid	One pot 20 min stirring at 25°C, one pot 90 min stirring at 95°C	• GO as precursor can yield more dispersed and smaller size AuNPs compared to sucrose precursor. • Synthesized graphenes possessed high intensity of carbon sp^2 electron formation. • I_D/I_G and $I_{D'}/I_G$ ratios for RGO-AA/AuNPs and RGO-DHA/AuNPs were 1.28 and 1.46, respectively.	This study

4. Conclusion

One pot synthesis of graphene nanocomposites, RGO-AA/AuNPs and RGO-DHA/AuNPs has been completed and characterized. This comparison evaluated chemical property and graphene quality of both methods. From UV-Vis and dynamic light scattering, the AuNPs of RGO-DHAA/AuNPs were found to be more dispersed, larger size and less stable due to physical morphology of reduced carbon precursor. Core level electron analysis indicated that oxygen functional groups of GO and sucrose has been successfully reduced by green agents.

Prominent sp^2 band peak was identified as a sign of structural change from sucrose to graphene. The relative intensity ratio of the I_D /I_G bands increased upon one pot reduction suggested the presence of graphene surface defects due to anchored AuNPs, consistent with other RGO/AuNPs studies. Sucrose may become alternative to Hummer's GO but in this study, more optimization is required to fully comprehend its processing capability. Even though the chemical pathway to transform sucrose to RGO is not clear, we hope the knowledge of these findings can highlight characteristics of graphene materials for diverse applications in the future.

Acknowledgments

We acknowledge financial assistance from Fundamental Research Grant Scheme (FRGS) provided by Ministry of Higher Education Malaysia under grant code FRGS/1/2020/STG07/UPNM/03/1.

References

[1] Brisebois P P and Siaj M 2020 *J. Mater. Chem. C* **8** 1517–1547

[2] Kamisan A I Demon S Z N Azmi A F M Abdullah N Kasim N A M Khim O K Noor S A M Yunus W M Z W Ros F C Shattar V. F. V. E. and Halim N. A. 2023, *EJSSNT* **21** 241-250

[3] Rowley-Neale S J Randviir E P Abo Dena A S and Banks C E 2018 *Appl. Mater. Today* **10** 218–226

[4] Mensing J P Poochai C Kerdpocha S Sriprachuabwong C Wisitsoraat A and Tuantranont A 2017 *Adv. Nat. Sci.: Nanosci. Nanotechnol.* **8** (2017) 033001

[5] Xu M Qi J Li F and Zhang Y 2018 *Nanoscale* **10** 5264–5271

[6] Al-Gaashani R Najjar A Zakaria Y Mansour S and Atieh M A 2019 *Ceram. Int.* **45** 14439–14448

[7] Kuang B Song W Ning M Li J Zhao Z Guo D Cao M and Jin H 2018 *Carbon* **127** 209–217

[8] Huang H H De Silva K K H Kumara G R A and Yoshimura M 2018 *Sci. Rep.* **8** 2–10

[9] Romero A Lavin-Lopez M P Sanchez-Silva L Valverde J L and Paton-Carrero A 2018 *Mater. Chem. Phys.* **203** 284–292

[10] Go S H Kim H Yu J You N H Ku B C and Kim Y K 2018 *Solid State Sci.* **84** 120–12511.

[11] Shelembe B, Mahlangeni N T and Moodley R 2019 Adv. Nat. Sci.: Nanosci. Nanotechnol. **10** 045002

[12] Vatandost E Saraei A G Chekin F Raeisi S N and Shahidi S A 2020 *Food Chem. X* **6** 100085

[13] Shittu K O Bankole M T Abdulkareem A S Abubakre O K and Ubaka A

U 2017 Adv. Nat. Sci.: Nanosci. Nanotechnol. **8** 035014

[14] De Silva K K H Huang H H and Yoshimura M 2018 Appl. Surf. Sci. 447 338–346

[15] Xu C. Shi X. Ji A Shi L Zhou C and Cui Y 2015 PLoS One 10 12

[16] Zhou C Zou H Li M Sun C Ren D and Li Y 2018 *Biosens. Bioelectron.* **117** 347–353 2018

[17] Nasir S Hussein M Z Yusof N A and Zainal Z 2017 *Nanomaterials* 7 7

[18] Faghiri F and Ghorbani F 2020 *Microchem. J.* **152** 104332

[19] Sankar S Lee H Jung H Kim A Ahmed A T A Inamdar A I Kim H Lee S Im H and Kim D Y 2017 *New J. Chem.* **41** 13792–13797

[20] Sujiono E H Zurnansyah Zabrian D Dahlan MY Amin B D Samnur Agus J 2020 *Heliyon* **6** e04568

[21] Hurtado R B Cortez-Valadez M J Aragon-Guajardo R Cruz-Rivera J J Martínez-Suárez F and Flores-Acosta M 2020 *Arab. J. Chem.* **13** 1633–1640

[22] Kotsidi M Gorgolis G Pastore Carbone M G Paterakis G Anagnostopoulos G Trakakis G Manikas A C Pavlou C Koutroumanis N Galiotis C 2023 *Nanoscale* **2** 5414–5428

[23] Rizzi V Laurenzana A Scavone F Frediani E Fibbi G Fanelli F Sibillano T Giannini C Fini P Cosma P Gubitosa J 2022 *Antioxidants* **11** 5

[24] Budlayan M L Lagare-Oracion J P Rosa L D Rodriguez M J Manigo J Alguno A Austria E Arco S Patricio J Deocaris C Basilia B and Capangpangan R 2021 *Adv. Nat. Sci.: Nanosci. Nanotechnol.* **12** 025007

[25] Jamkhande P G Ghule N W Bamer A H and Kalaskar M G 2019 *J. Drug Deliv. Sci. Technol.* **53** 101174

[26] Kumar N Setshedi K Masukume M and Ray S S 2022 Carbon Lett. **32** 1031–1046

[27] Li B Jin X Lin J and Chen Z 2018 *J. Clean. Prod.* **189** 128–134

[28] Sethi M. Bantawal H Shenoy U S and Bhat D K. 2019 *J. Alloys Compd.* **799** 256–266

[29] Hauswirth A Köhler R ten Bosch L Avramidis G and Gerhard C 2022 *Foods* **11** 1–13

[30] Faniyi I O Fasakin O Olofinjana B Adekunle A S Oluwasusi T V Eleruja M A and Ajayi E O B 2019 *SN Appl. Sci.* **1** 1–7

[31] Tegafaw T Xu W Ahmad M W Baeck J S Chang Y Bae J E Chae K S Kim T J and Lee G H 2015 *Nanotech.* **26** 365102

[32] Lafuente M Sanza D Urbiztondoc M Santamaría J Pina M P Mallada R 2020 *J. Hazard. Mater.* **384** 121279

[33] Wang J, Zhang S, Zhou J, Liu R, Du R, Xu H, Liu Z, Zhang J and Liu Z 2014 *Phys. Chem. Chem. Phys.* **16** 11303

[34] King A A K, Davies B R, Noorbehesht N, Newman P, Church T L, Harris A T, Razal J M and Minett A I 2016 *Sci. Rep.* **6**, 19491

[35] Gao J Liu F Liu Y Ma N Wang Z and Zhang X 2010 *Chem. Mater.* **22** 2213–2218

[36] Palomba M Carotenuto G and Longo A 2022 *Mater.(Basel)* **15** 18

[37] Yousefimehr F Jafarirad S Salehi R and Zakerhamidi M S 2021 *Sci. Rep.* **11** 1–13